MODELLED V-I PERFORMANCE OF A ^{3}HE COMPOSITE BOLOMETER DETECTOR

B. G. Gom and D. A. Naylor

Department of Physics
University of Lethbridge
Lethbridge, Alberta
Canada
T1K 3M4

Received

The V-I characteristics of a ^{3}He-cooled, composite bolometer detector designed for submillimetre astronomy are modelled. The modelling yields detector parameters that cannot be measured directly. The system NEP predicted from theoretical V-I equations is found to agree with the measured noise values. The calculated dynamic thermal conductance and the electrical responsivity are found to deviate from the standard model at low temperatures.

Keywords : Bolometer, Submillimetre

1. Introduction

Measurements of the bolometer voltage as a function of bias current and radiant power loading provide a simple method of determining the performance of a bolometer [1,2,3]. By fitting theoretical curves to the V-I data, one can obtain values for parameters that would otherwise be difficult to measure, such as the thermal conductance, radiant loading, and detector temperature. From analysis of the V-I curves and the detector frequency response, the NEP of the bolometer can be calculated as a function of bias current, which in turn provides a means of optimising the bias current for a given loading condition.

2. Bolometer Theory

A schematic of the heat flow through a bolometer is shown in Figure 1a. Radiation incident on the bolometer, from all sources, is represented by a radiant power loading, Q, while electrical power dissipated in the bolometer is represented by P. In thermal equilibrium the power flowing into the bolometer is equal to the power flowing out through the thermal link, W, given by:

$$W = P + Q \tag{1}$$

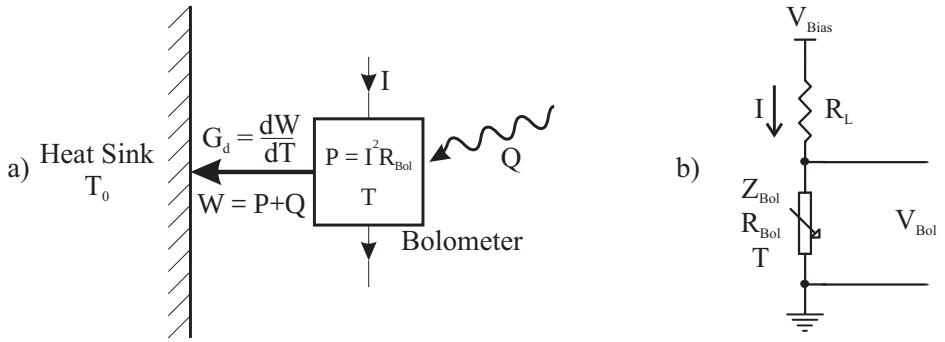

Figure 1 : Schematics of the equivalent (a) thermal and (b) electrical bolometer circuits.

The steady state thermal conductance, G, of a thermal link, depends on the temperature gradient, composition, and geometry of the link. In thermal equilibrium with a heat sink of temperature T_0, the heat flow through the link, W, is given by:

$$W = G_{(T,T_0)} \cdot (T - T_0) \tag{2}$$

where T is the bolometer temperature.

The dynamic thermal conductance, G_d, is defined as the rate change of heat flow caused by a change in temperature:

$$G_d = \frac{dW}{dT} \tag{3}$$

Under constant radiant loading, the temperature of the bolometer varies only with a change in the electrical power dissipated as a result of a change in the bias current, and the dynamic thermal conductance reduces to:

$$G_d = \frac{dP}{dT} \tag{4}$$

Following other authors [2,4,5], we assume that the steady state thermal conductance can be expressed as a simple power law:

$$G = G_0 \left(\frac{T}{T_0} \right)^{\beta} \tag{5}$$

$$\therefore \quad W = G \cdot (T - T_0) = G_0 \left(\frac{T}{T_0} \right)^{\beta} (T - T_0)$$

where G_0 is the thermal conductance at the sink temperature, $T=T_0$, and β is a material dependent parameter, ~1 for metals and ~3 for dielectrics.

Given any functional form for the thermal conductance, the electro-thermal behaviour of the bolometer can be modelled completely. The first step is to derive an expression for the thermal conductance in terms of directly measurable electrical quantities. An equivalent electrical circuit for a typical bolometer is shown in Figure 1b,

where the bolometer is represented by a temperature dependent resistance, R_{Bol}. A bias voltage, V_{Bias}, applied across a load resistor, R_L, in series with the bolometer, creates a bias current, I. R_L is chosen to be much larger than R_{Bol} so that the bias current has a minimal dependence on R_{Bol}. The bolometer signal is then measured as the voltage drop across the bolometer, V_{Bol}. The dynamic impedance of the bolometer is defined as:

$$Z = \frac{dV_{Bol}}{dI} \tag{6}$$

The resistance of a Ge:Ga bolometer crystal as a function of doping level has been studied by Haller [6] and can be expressed in the empirical form:

$$R_{Bol} = R^* e^{\sqrt{T_g/T}} \tag{7}$$

where T_g is a material dependent parameter, and R^* depends on both the material and geometry of the crystal. For the material used in our detectors (Haller NTD #13), R^* = 7.56 Ω and T_g = 62.6 K.

Equation (7) can be solved for the bolometer temperature, T, and written in terms of V_{Bol} and I as:

$$T = \frac{T_g}{\left(\ln \frac{R_{Bol}}{R^*}\right)^2} = \frac{T_g}{\left(\ln \frac{V_{Bol}}{IR^*}\right)^2} \tag{8}$$

The electrical power dissipated in the bolometer is:

$$P = V_{Bol} I = I^2 R_{Bol} = \frac{{V_{Bol}}^2}{R_{Bol}} \tag{9}$$

Equations (6), (7) and (9) can be manipulated to express the dynamic thermal conductance as [7]:

$$G_d = \frac{dP}{dT} = I^2 \frac{dR_{Bol}}{dT}\left(\frac{Z + R_{Bol}}{Z - R_{Bol}}\right) \tag{10}$$

The heat flow through a bolometer is analogous to the flow of electrical current through an RC circuit. As a result, a thermal time constant for the bolometer can be defined in terms of its thermal capacitance, C, as:

$$\tau \equiv \frac{C}{G_d} \tag{11}$$

Zwerdling [8] has shown that the electro-thermal interaction between the heating of the bolometer from the absorbed radiation, and the resulting change in dissipated electrical power, acts to increase the apparent thermal conductivity. The resulting effective thermal conductance, G_e, is given by:

$$G_e = G_d - I^2 \frac{dR_{Bol}}{dT}\left(\frac{R_L - R_{Bol}}{R_L + R_{Bol}}\right) \tag{12}$$

where the term in the brackets is referred to as the static electro-thermal interaction function.

As a result of the change in thermal conductance, the measured time constant of the electrical detector signal differs from the physical time constant when the detector views a modulated source of radiation. This effective time constant, τ_e, is given by [8]:

$$\tau_e \equiv \frac{C}{G_e} = \frac{C}{I^2 \dfrac{dR_{bol}}{dT}} \frac{\left(R_{Bol} + R_L\right)\left(Z - R_{Bol}\right)}{2R_{Bol}\left(Z + R_L\right)} \tag{13}$$

$$\therefore \quad \frac{\tau_e}{\tau} = \frac{Z + R_{Bol}}{2R_{Bol}} \frac{R_{Bol} + R_L}{Z_{Bol} + R_L} \tag{14}$$

In the special case when Z is zero (and $R_L >> R_{Bol}$), the electro-thermal interaction acts to effectively double the frequency response of the detector.

Using Equations (1) and (3), the electrical power can be rewritten as:

$$P = W - Q = \int_{T_0}^{T} G_d \, dT - Q \tag{15}$$

Equations (7), (9), and (15) can now be combined to yield the general parametric bolometer voltage and bias current equations:

$$V_{Bol} = \sqrt{\left[\int_{T_0}^{T} G_d \, dT - Q\right] \cdot R^* e^{\sqrt{T_g / T}}} \qquad I = \sqrt{\frac{\int_{T_0}^{T} G_d \, dT - Q}{R^* e^{\sqrt{T_g / T}}}} \tag{16}$$

If the thermal conductance can be described by a power law (Equation (5)), then Equation (15) becomes:

$$P = G_0 \left(\frac{T}{T_0}\right)^{\beta} \left(T - T_0\right) - Q \tag{17}$$

and Equations (16) become:

$$V_{Bol} = \sqrt{\left[G_0 \left(\frac{T}{T_0}\right)^{\beta} (T - T_0) - Q\right] \cdot R^* e^{\sqrt{T_g / T}}} \qquad I = \sqrt{\frac{G_0 \left(\frac{T}{T_0}\right)^{\beta} (T - T_0) - Q}{R^* e^{\sqrt{T_g / T}}}} \tag{18}$$

Equations (18) form the basis for our modelling. By fitting these equations to the experimental data, the values of G_0, T_0, and Q can be determined.

3. Measured V-I Characteristics

The data presented here were obtained with a new dual polarizing bolometer detector system that has been developed for use with a polarizing Fourier transform spectrometer to conduct broadband, intermediate resolution, astronomical spectroscopic observations at submillimetre wavelengths [9,10]. The V-I data were collected by recording the bolometer voltage, V_{Bol}, as the bias current was varied by manually adjusting the bias

voltage, V_{Bias}, from 0 to ~4 volts. Data were obtained for the detector system viewing hot (338 K), ambient (290 K), and liquid nitrogen (73 K) blackbody sources, and a blanked off filter position corresponding to the least possible radiant loading (4 K).

Although the detector system employs a fully differential electronic design to eliminate common mode noise (shown schematically in Figure 2), the circuit is equivalent to that of Figure 1b. The resistance of the bolometer is determined from the bolometer voltage, V_{Bol}, and the load resistance, R_L, as:

$$R_{Bol} = \frac{V_{Bol} \cdot R_L}{V_{Bias} - V_{Bol}} \tag{19}$$

The bias voltage is then converted to bias current by:

$$I = \frac{V_{Bias}}{R_L + R_{Bol}} \tag{20}$$

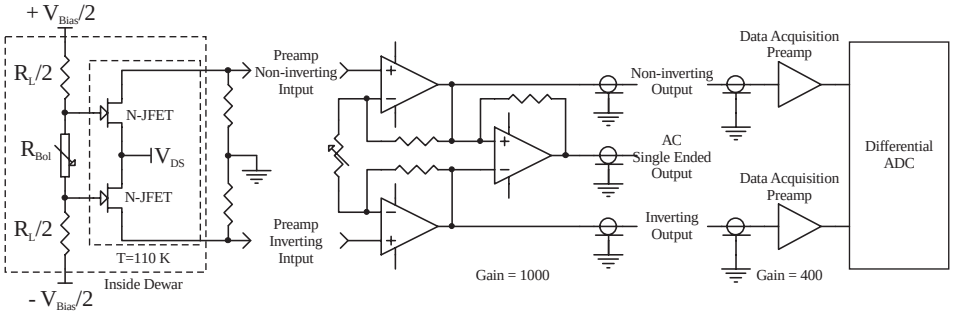

Figure 2. Simplified schematic of the differential bolometer circuit, preamp and data acquisition system.

In our design, the measured detector output voltage, V, is related to the bolometer voltage, V_{Bol}, by:

$$V_{Bol} = \frac{V}{Gain} - Offset \tag{21}$$

where account is taken of the gain and offset of the amplifiers shown in Figure 2 (the offset is determined when $V_{Bias} = 0$). The bias current then becomes:

$$I = \frac{V_{Bias} - \left(\frac{V}{Gain} - Offset \right)}{R_L} \tag{22}$$

The bolometer voltage can now be plotted as a function of bias current. Figure 3 shows an example of the measured V-I curves for the 850 μm band, one of six available filter bands in the detector system [9,10]. The uppermost curve represents the lowest radiant loading in which the detector views a 4 K source. In order, subsequent curves represent the detector viewing liquid nitrogen, ambient, and hot blackbody sources.

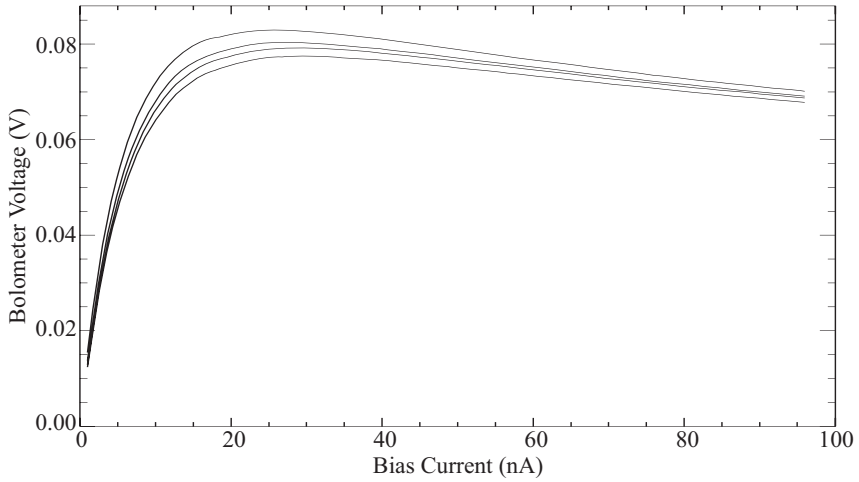

Figure 3. Measured V-I curves. In order from top to bottom, the curves represent the detector viewing 4 K, 73 K, 290 K and 338 K sources, respectively.

The V-I curves can be analysed to yield values for the thermal conductance, G_0, the heat sink temperature, T_0, and the radiant power loading, Q of the bolometer, parameters which, in our case, cannot easily be determined by other means.

One method is to assume the simple power law form for the thermal conductance (Equation (5)), and to fit the theoretical V-I equations (Equations (18)) to the experimental data by varying G_0, T_0, and Q. Since the experimental data are irregularly gridded and contain random jitter in both the voltage and current coordinates, a custom IDL [11] routine was written to fit the measured data to the theoretical V-I equations. The routine explores the 3-dimensional parameter space defined by G_0, T_0, and Q. Theoretical V-I curves are generated at regular intervals spanning the variable space and compared with the experimental data to yield a χ^2 statistic. Reasonable values are chosen for the initial range of each parameter and the resulting data cube is then visualized in IDL to verify that the global minimum χ^2 is within the set parameter ranges. The parameter ranges and calculation intervals are iteratively decreased until an appropriate convergence limit has been reached. Once the best fit is found, the radiant loading for the liquid nitrogen, ambient and hot blackbody sources can be determined by fixing the values of G_0 and T_0, and repeating the least squares fitting procedure.

Figure 4 shows the measured V-I data (symbols) and the theoretical best fit (line) for the detector viewing a 4 K source. A summary of the parameters determined by the fitting procedure is given in Table 1. The uncertainties listed correspond to the step sizes of the array of parameter values used in the fitting routine, when convergence has been reached. The simple theoretical model shows excellent agreement with the measured data, and does not require invoking an electric field effect in the bolometer crystal as was considered by Holland [12].

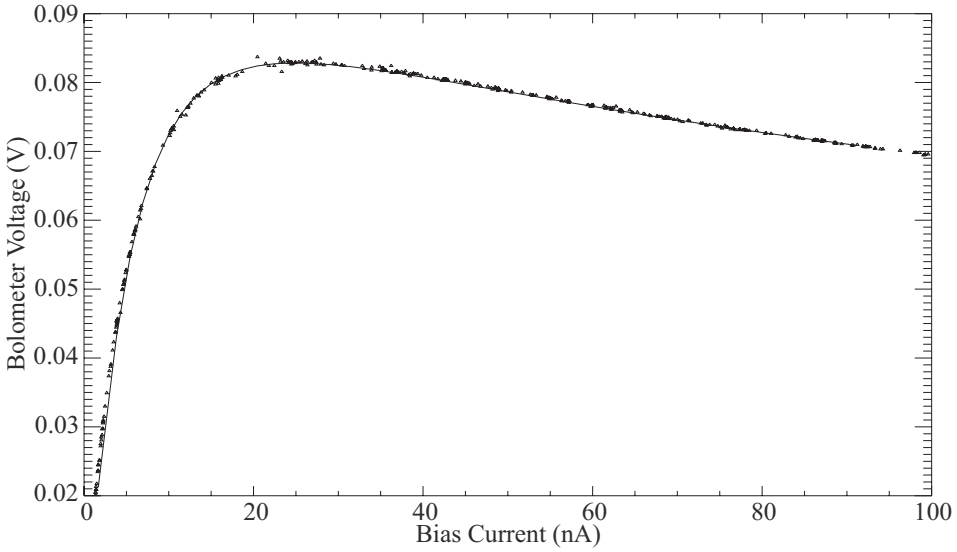

Figure 4. Theoretical V-I fit (line) to the measured data (symbols), for a 4 K source.

Fit Parameter	Value	Uncertainty
G_0 (nW/K)	24.55	0.1
T_0 (K)	0.300	0.0003
Q (pW)	89.2	1.5

Table 1.

A second method of deriving G_0 and T_0, is to determine the temperature dependence of G_d, and the zero load temperature of the bolometers directly from the V-I data.

The measured V-I data can be substituted into Equation (8) to produce the plot of the bolometer temperature as a function of bias current shown in Figure 6. The bolometer is seen to reach a minimum temperature of 0.293 K (at zero bias current), which sets an upper limit on the heat sink temperature. This value is slightly less than that listed in Table 1, but, in the following analysis, we assume that the heat sink temperature, T_0, does not differ significantly from this value. Both values, however, are consistent with the temperature of ~ 0.3 K measured by the GR100 [13] Ge temperature sensor mounted on the cold stage which supports the bolometer housing (see [10]).

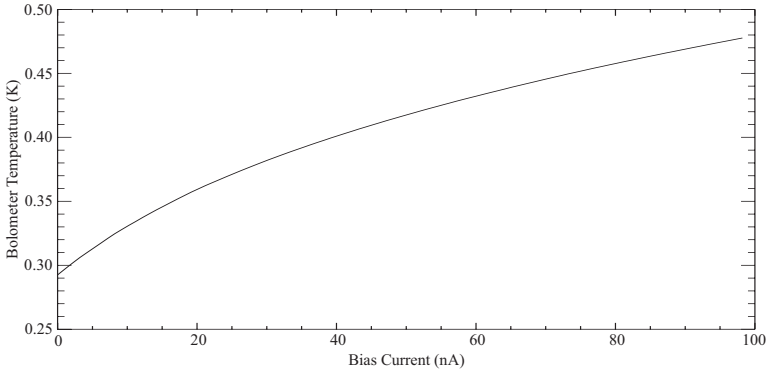

Figure 6. Measured bolometer temperature as a function of bias current, for a 4 K source.

The temperature dependence of the dynamic thermal conductance can be determined from the experimental data by taking the numerical derivative of $P=I^2R$ with respect to T, and compared to the model thermal conductance given by:

$$G_d = \frac{d}{dT}\left(G_0 \left(\frac{T}{T_0} \right)^{\beta} \left(T - T_0 \right) \right) = G_0 \left(\frac{2T}{T_0} - 1 \right) \qquad \text{using } \beta = 1 \text{ for a metal link} \qquad (23)$$

Figure 5 shows the experimental G_d data (symbols) and the nonlinear least-squares best fit of the model thermal conductance given by Equation (23) (line).

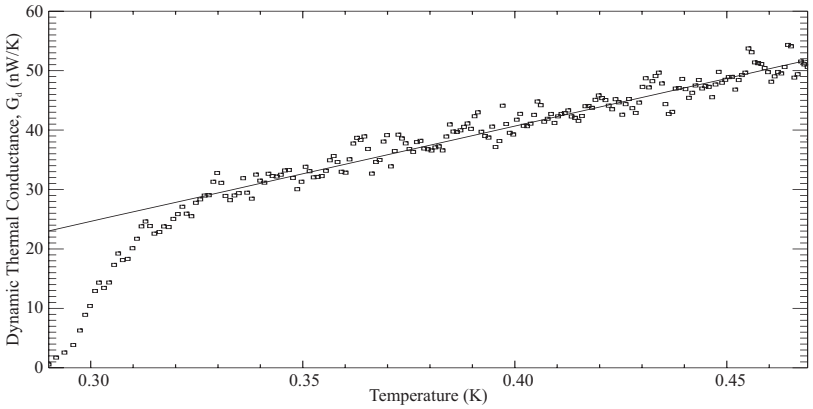

Figure 5. Temperature dependence of the dynamic thermal conductance, G_d, calculated from V-I data (symbols) and the theoretical model (line), for a 4 K source.

It can be seen that the model thermal conductivity curve fits the experimentally derived values well except at low temperatures, where the actual thermal conductance falls away more rapidly. Although the experimental data are noisy, the general shape of the curve is the same for the four, independently measured, loading conditions, indicating

that the change in slope at low bias current is not due to mathematical propagation of the random jitter in the measured V-I data. (Moreover, an error in the amplifier offset or gain cannot account for this effect.) Since a thermal conductivity of zero at $T=T_0$ is nonphysical, this points to a possible deficiency in the model of thermal conductance at low temperature gradients. We can, however, fit Equation (23) to the experimental G_d data for temperatures above 0.33 K to obtain a value for G_0 of 23.5 nW/ K. While the values determined by these two methods (Tables 1 and 2) are in general agreement, those in Table 1 are less robust since they necessarily include the low temperature data which is shown to deviate from the model.

Fit Parameter	Value	Uncertainty
G_0 (nW/K)	23.5	0.004
T_0 (K)	0.293	0.001

Table 2.

The heat capacity of the bolometer, C, can now be determined from Equation (11) using the thermal conductance from Table 2, and the detector physical time constant,τ. The effective detector time constant was measured to be 3 ms, which, under the operating bias conditions corresponds to a physical time constant of 6 ms (Equation (14)). The resulting heat capacity is 141 pJ/K, which is within the range set by manufacturing tolerances.

4. Responsivity

The responsivity of a detector is defined as the detector voltage produced by a given radiant power, $\Re = \frac{dV_{Bol}}{dQ}$, and can be determined from the V-I curves (electrical responsivity), and independently from optical measurements (optical responsivity).

The theoretical electrical responsivity can be evaluated from the derivative of Equations (18) (using $\beta = 1$) as:

$$\Re_0 = -\frac{1}{2}\sqrt{\frac{T_0 R^*}{G_0 T(T-T_0)-QT_0}}\cdot e^{\sqrt{T_g/4T}} \tag{24}$$

For a detector with a single time constant, the zero frequency responsivity, $\Re_0$, is attenuated with increasing frequency according to [7]:

$$\Re_{(\omega)} = \Re_0 \cdot \left(1+\omega^2\tau_e^2\right)^{-1/2} \tag{25}$$

The electrical responsivity can also be calculated directly from the measured V-I data using the derivation of Jones [1]:

$$\Re_{(\omega)} = \frac{R_L}{2IR_{Bol}}\cdot\frac{Z_{(\omega)}-R_{Bol}}{Z_{(\omega)}+R_L} \tag{26}$$

Figure 7 shows the nonlinear least-squares best fit of the theoretical responsivity (Equation (24)) to the the experimentally derived responsivity (Equation (26)). The fact that the theoretical curve (solid line) deviates from the experimental data (symbols) again points to deficiencies in the model at low temperatures (ie. low bias currents). Above 20 nA, however, there is general agreement between the responsivity curves.

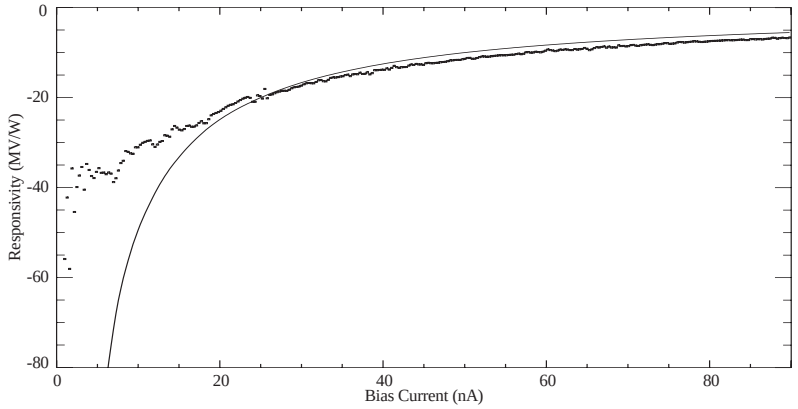

Figure 7. Measured electrical responsivity (symbols) and theoretical model (line), for a 4 K source.

The optical responsivity, $\Re = \frac{\Delta V_{Bol}}{\Delta Q}$, can be determined directly from the voltage difference between two V-I curves given the difference in the radiant power loading on the bolometer, ΔQ. Figure 8 shows an example of the high quality of the agreement between the optical (symbols) and electrical (line) responsivities calculated from Equation (26).

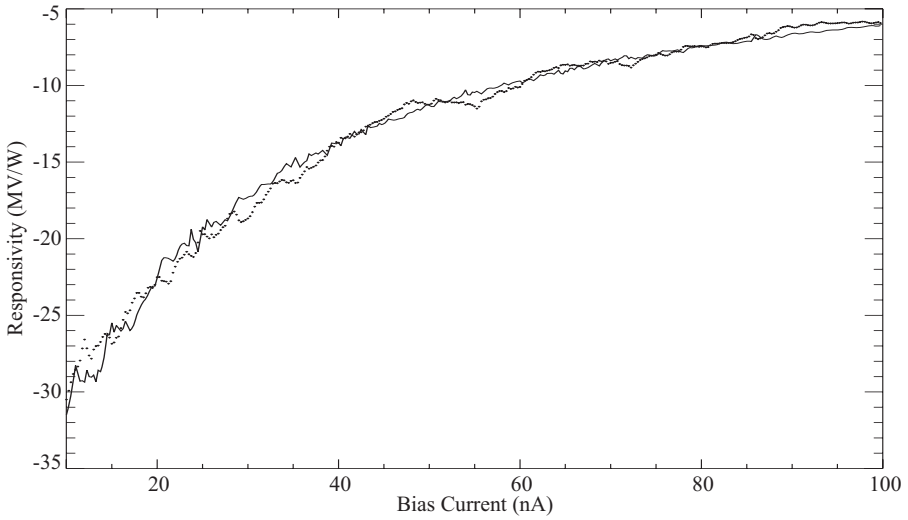

Figure 8. Fit optical (symbols) and electrical (line) responsivities, for a 4 K source.

5. Theoretical Noise Performance

The total detector noise equivalent power (NEP) can be expressed as:

$$NEP_{Total}^2 = NEP_{Photon}^2 + NEP_{Phonon}^2 + NEP_{Johnson}^2 + NEP_{Load}^2 + NEP_{Preamp}^2 + NEP_{Ex}^2 \tag{27}$$

The first term represents the absolute minimum achievable NEP set by the photon background [7], given by:

$$NEP_{Photon}^2 = A\Omega \cdot a\varepsilon f \cdot \frac{4k^5T^5}{h^3c^2} \int_x \frac{x^4}{e^x - 1}\left(\frac{a\varepsilon f}{e^x - 1} + 1\right)dx \tag{28}$$

$$where \quad x = \frac{h\nu}{kT}$$

where $A\Omega$ is the detector optical throughput, a is the absorptivity of the detector, ε is the the emissivity of the source, f is the transmissivity of the optics, k is Boltzmann's constant, h is Planck's constant, c is the speed of light, ν is the radiation frequency, and T is the temperature of the source.

The second term represents the noise produced in the bolometer as a result of random fluctuations in heat flow between the bolometer and the heat sink. This phonon NEP can be expressed as a Taylor series, using the notation $\Delta = 1 - T_0/T$ [7], as:

$$NEP_{Phonon}^2 = 4kGT^2\left[1 - \left(\frac{\beta}{2} + 1\right)\Delta + \left(\frac{(\beta+2)(3\beta+2)}{12}\right)\Delta^2 - \cdots\right] \tag{29}$$

The third term represents the Johnson noise of the bolometer, taking into account the electro-thermal feedback from the bias network [7]:

$$NEP_{Johnson}^2 = 4kTP\left|\frac{Z + R_{Bol}}{Z - R_{Bol}}\right|^2 \left(1 + \omega^2\tau^2\right) \tag{30}$$

The fourth term represents the Johnson noise associated with the load resistors [7], neglecting the noise contribution from the bias voltage supply (which is ~ 0.2 $nV/\sqrt{Hz}$ at 50 Hz), this becomes:

$$NEP_{Load}^2 = \frac{4kT_L}{R_L}\left|\frac{2ZI}{\frac{Z}{R_{Bol}} - 1}\right|^2 \left[1 + \omega^2\tau^2\left(\frac{Z + R_{Bol}}{2Z}\right)^2\right] \tag{31}$$

The fifth term represents noise associated with the differential amplifier which can also be expressed in the terms of a NEP. The JFETs (IFN146 [14]), in Figure 2, are the primary source of amplifier noise. There are two components of the JFET noise current: a thermal component of 0.08 $fA/\sqrt{Hz}$, and a shot component of 0.4 $fA/\sqrt{Hz}$. In addition, there are two components of the JFET noise voltage: Flicker noise (thought to be due to surface defects in the device), and Johnson noise produced in the channel resistance. The total JFET noise voltage, e_{nJFET}, is ~ 0.6 $nV/\sqrt{Hz}$ at 50 Hz [10]. Following the notation of

Mather [7], when the electro-thermal interaction of the bias network is included, the total preamp NEP contribution becomes:

$$NEP_{Preamp}^2 = i_{nJFET}^2 \left| \frac{2ZI}{\frac{Z}{R_{Bol}} - 1} \right|^2 \left[1 + \omega^2 \tau^2 \left(\frac{Z + R_{Bol}}{2Z} \right)^2 \right] + \frac{e_{nJFET}^2}{\left| \Re^2(\omega) \right|} \tag{32}$$

$$where \quad i_{nJFET} = \sqrt{i_{nThermal}^2 + i_{nShot}^2} \approx 0.4 \; fA/\sqrt{Hz}$$

The final term represents all forms of excess noise which are not easily modelled. When using the detector for astronomical observations, the most common forms of excess noise are: Microphonics, electromagnetic interference, varying atmospheric transmission and cosmic rays. While the differential electronic design virtually eliminates microphonic and electrical noise the latter two sources are unavoidable.

The noise components of Equation (27) have been computed from the V-I data. Figure 9 shows plots of the total detector NEP for a signal frequency of 50 Hz. Excess noise is not included in the model.

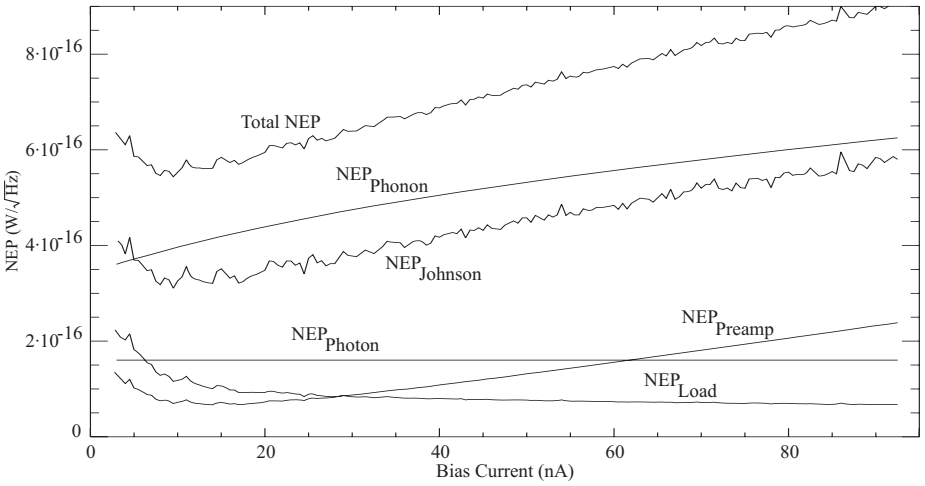

Figure 9. Contributions to the total NEP from the components given in Equation (27) for a 73 K source.

The theoretical minimum NEP for a bolometer can be expressed as [4]:

$$NEP_{min} = aT_0\sqrt{kG_0} + bQ\sqrt{k/G_0} \tag{33}$$

where, a and b are dependent on the bolometer material and temperature. For our detector, $a = 2.52$ and $b = 3.31$. Using the values for G_0, T_0, and Q determined by the V-I fitting procedure (Table 1), the theoretical minimum NEP is $4.5 \cdot 10^{-16}$ $W/\sqrt{Hz}$, which is consistent with the theoretical NEP value calculated from the V-I data (Figure 9) and from directly measured noise values [10].

6. Conclusion

Measurements of the V-I characteristics of a ^{3}He-cooled, composite bolometer detector have been used as inputs to a theoretical bolometer model to yield values for the thermal conductance, G_0, heat sink temperature, T_0, radiant power loading, Q, electrical and optical responsivity, $\Re$, and NEP. The model, which uses a simple power law form for the thermal conductance, provides a good fit to the measured V-I data. The simple and robust fitting algorithm yields detector parameter values consistent with the design. While the thermal conductance and responsivity derived from the measured data depart from the model predictions at low temperatures (bias currents), indicating that deficiencies still exist in the simple model, the model provides reliable NEP values and can be used to determine the optimum bias current settings for a given radiant loading.

7. Acknowledgements

The authors acknowledge support from NSERC.

8. References

[1] R. C. Jones, "General Theory of Bolometer Performance", *J. Opt. Soc. Am.*, **43**, 1-14, 1953.

[2] G. Chanin and J. P. Torre, *J. Opt. Soc. Am. A.*, **1**, 412-419, 1984.

[3] F. J. Low, *J. Opt. Soc. Am.*, **51**, 1300-1304, 1961.

[4] M. J. Griffin and W. S. Holland, "The Influence of Background Power on the Performance of an Ideal Bolometer", *Int. J. of Infrared and Millimetre Waves*, **9**, No. 10, 861, 1988.

[5] J. C. Mather, "Bolometers: ultimate sensitivity, optimization, and amplifier coupling", *Appl. Opt.*, **23**, No. 4, 584-588, 1984.

[6] E. E. Haller, "Physics and Design of Advanced IR Bolometers and Photoconductors", *Infrared Physics*, **25**, 257, 1985.

[7] J. C. Mather, "Bolometer Noise: Nonequilibrium Theory", *Appl. Opt.*, **21**, No. 6, 1125-1129, 1981.

[8] S. Zwerdling, R. A. Smith, and J. P. Theriault, "A Fast, High-Sensitivity Bolometer Detector for the Very-Far Infrared", *Infrared Physics*, **8**, 271-336, 1968.

[9] D. A. Naylor, B. G. Gom, P. A. R. Ade, and J. E. Davis, "Polarizing Fourier transform spectrometer for astronomical spectroscopy at submillimeter and mid-infrared wavelengths", *Proc. SPIE*, **2198**, 703-714, 1994.

[10] D. A. Naylor, B. G. Gom, P. A. R. Ade, and J. E. Davis, "Design and performance of a dual polarizing detector system for broadband astronomical spectroscopy at submillimetre wavelengths", *Rev. Sci. Instrum.*, Submitted.

[11] Research Systems, Inc., 4990 Pearl East Circle, Boulder, Colorado, 80301, USA.

[12] W. S. Holland, *Design and Development of Bolometric Detector Systems*, Ph. D. Thesis, QMW, London, UK, 1991.

[13] Lakeshore Cryotronics Inc., 64 East Walnut Street, Westerville, Ohio, 43081-2399, USA.

[14] InterFet Corporation, 1000 North Shiloh Road, Garland, Texas, 75042, USA.